Supporting Information

Hormoz et al. 10.1073/pnas.1504407112

SI Text

Overview

SI Text contains the following sections. In *Example* and *Higher-Order Correlations*, we discuss the operator product expansion and work out an example calculation of a tree correlation function. *Connected Correlators* defines the notion of connected correlators. *Perturbative Corrections* contains the explicit calculation of the perturbative corrections to the noninteracting minimal model when sibling interactions are added. In *Broken Detailed Balance*, we discuss the signature of broken detailed balance on the correlation functions. In *Statistical Analysis*, we present the P values for the deviation of the experimentally measured two-point correlation functions from the prediction of the minimal model. *Finite Size Fluctuations* deals with finite size fluctuations and presents an estimate of the number of trees required to obtain statistically significant correlation functions. In *Analysis of Pvd*, we show that the distribution of Pvd states in the population is stationary. *Simulations* discusses in detail the simulations used for our analysis. *Hyperbolic Trees* contains our construction of the Bethe lattice in hyperbolic space.

Example: Calculating a Correlation Function

It is instructive to explicitly compute a correlation function on a tree. The following example demonstrates how to introduce structure constants at the vertices and eigenvalue propagators on the edges to evaluate a correlation function (see also ref. 1). Consider the following tree of interest—the irrelevant branches have been discarded. We would like to evaluate the correlation function of observing the four propagation modes α, β, γ, and δ on the boundary. The input mode from the root is 0—the equilibrium mode with eigenvalue 1.

We evaluate the correlation function as follows: For each edge, insert a factor λ_i where i is the mode propagating on the edge. For each vertex with three edges, insert a factor of a structure constant $C_{\alpha\beta\delta}$. Edges that connect two internal vertices correspond to the internal propagation modes (μ and ν in Fig. S1), which are summed over. Above example yields,

$$\hat{G}_{\alpha\beta\gamma\delta} = \lambda_\alpha\lambda_\beta \sum_\mu C_{\mu\alpha\beta}\lambda_\mu^4 \sum_\nu C_{0\mu\nu}\lambda_\nu^3 C_{\nu\gamma\delta}\lambda_\gamma^2\lambda_\delta^2. \quad \text{[S1]}$$

Following the minimal model, we can use the diagonal form of the two point correlation functions, $C_{0\mu\nu} = \delta_{\mu,\nu}$.

$$\hat{G}_{\alpha\beta\gamma\delta} = \lambda_I\lambda_H \sum_\mu C_{\mu\alpha\beta}\lambda_\mu^7 C_{\mu\gamma\delta}\lambda_\gamma^2\lambda_\delta^2. \quad \text{[S2]}$$

The above correlation functions can be converted to correlation functions in space of phenotypic states by performing a transformation.

Higher-Order Correlation Functions and the Operator Product Expansion

In conformal field theories, higher-order correlators can be related to lower-order correlators using the Operator Product Expansion (OPE) (2). Following Harlow et al. (1), one can show that the same general relation holds for the Detailed Balanced Markovian dynamics on the tree.

Consider the following n-point correlation function involving nodes x and y whose common ancestor is u generations back.

$$\hat{G}^{(n)}_{\alpha\beta\gamma\dots} = \langle \phi^\alpha(x)\phi^\beta(y)\phi^\gamma(z)\dots\rangle = \sum_\gamma C_{\alpha\beta\delta}\lambda_\alpha^u\lambda_\beta^u\lambda_\delta^{-u}\langle \phi^\delta(x)\phi^\gamma(z)\dots\rangle \quad \text{[S3]}$$

$$= \sum_\gamma C_{\alpha\beta\delta}\lambda_\alpha^u\lambda_\beta^u\lambda_\delta^{-u}\hat{G}^{(n-1)}_{\delta\gamma\dots}. \quad \text{[S4]}$$

Defining the distance between nodes x and y as $|x-y| = e^u$ and the scaling dimensions as $\Delta_\alpha = -log\lambda_\alpha$ converts this relation into the form

$$\langle \phi^\alpha(x)\phi^\beta(y)\phi^\gamma(z)\dots\rangle = \sum_k \frac{C_{\alpha\beta\gamma}}{|x-y|^{\Delta_\alpha+\Delta_\beta-\Delta_\delta}}\langle \phi^\delta(x)\phi^\gamma(z)\dots\rangle, \quad \text{[S5]}$$

which is exactly the form of OPE derived in conformal field theories (2, 3).

Connected Correlators

Recall that connected pair-wise correlators are defined as

$$g^{(2)}_{mn}(u) = G^{(2)}_{mn}(u) - p_m p_n, \quad \text{[S6]}$$

where p_m is the stationary probability of phenotype m. Similarly, the three-point connected correlators take the form

$$g^{(3)}_{lm,n}(u,v) = G^{(3)}_{lm,n}(u) - p_n g^{(2)}_{lm}(u) - p_m g^{(2)}_{ln}(v) - p_l g^{(2)}_{mn}(v) - p_l p_m p_n, \quad \text{[S7]}$$

Connected correlators have no contribution from independent fluctuations and decay to zero when the joint distribution of the nodes factorizes.

It is also convenient to subtract out the equilibrium component from the transition matrix, defining the "propagator" describing approach to equilibrium

$$\mathbf{T}_u(m|n) = T_u(m|n) - p_m = p_m^{1/2}p_n^{-1/2}\sum_{\alpha=1}(\lambda_\alpha)^u\phi_m^\alpha\phi_n^\alpha. \quad \text{[S8]}$$

This is useful because connected correlators $g^{(2)}_{mn}$ and $g^{(3)}_{lmn}$ can be found by substituting $\mathbf{T}$ for T in the corresponding expressions for $G^{(2)}_{mn}$ and $G^{(3)}_{lmn}$.

Perturbative Corrections to the Conformal Limit

We calculate explicitly the leading order corrections to the conformal limit for $M = 3$. In the main text, we showed that with no interactions, $\tilde{\Gamma}_0(\alpha,\beta|\delta) = \lambda_\alpha\lambda_\beta C_{\alpha\beta\delta}$. We account for interactions by adding a correction to the structure constants,

$$\tilde{\Gamma}(\alpha,\beta|\delta) = \lambda_\alpha\lambda_\beta\left(C_{\alpha\beta\delta} + D_{\alpha\beta\delta}\right). \quad \text{[S9]}$$

Our goal is to fit the corrections $D_{\alpha\beta\delta}$ to the observed correlation functions.

The two-point correlation function with interactions can be represented in a matrix form.

$$\mathcal{C}_{\alpha\beta}(u) = \begin{pmatrix} 1 & 0 & 0 \\ 0 & (1+D_{110})\lambda_1^{2u} & D_{120}\lambda_1^u\lambda_2^u \\ 0 & D_{120}\lambda_1^u\lambda_2^u & (1+D_{220})\lambda_2^{2u} \end{pmatrix}. \quad \text{[S10]}$$

An observer, unaware of local interactions, would diagonalize the above matrix and infer a set of effective eigenvalues and eigenvectors. The eigenvalues are, to zeroth order, the minimal model eigenvalues—those of a transition matrix constructed from the marginal distribution of Γ—plus a correction that vanishes with increasing u.

$$\tilde{\lambda}_0 = \lambda_0 = 1$$

$$\tilde{\lambda}_1 = \lambda_1(1+D_{110})^{\frac{1}{2u}} + \ldots = \lambda_1\left(1+\frac{1}{2u}D_{110}\right) + \ldots$$

$$\tilde{\lambda}_2 = \lambda_2\left(1+D_{220}-\frac{D_{120}^2}{1+D_{110}}\right)^{\frac{1}{2u}} + \ldots$$

$$= \lambda_2\left(1+\frac{1}{2u}D_{220}-\frac{1}{2u}\frac{D_{120}^2}{1+D_{110}}\right) + \ldots.$$

The eigenvectors (propagating modes) to the first-order correction take the following form in the noninteracting basis:

$$\tilde{\phi}^0 = \begin{pmatrix} 1 \\ 0 \\ 0 \end{pmatrix} \qquad \text{[S11]}$$

$$\tilde{\phi}^1 = \begin{pmatrix} 0 \\ 1 \\ \dfrac{D_{120}\left(\dfrac{\lambda_2}{\lambda_1}\right)^u}{D_{110}+1} \end{pmatrix} + \ldots \qquad \text{[S12]}$$

$$\tilde{\phi}^3 = \begin{pmatrix} 0 \\ -\dfrac{D_{120}\left(\dfrac{\lambda_2}{\lambda_1}\right)^u}{D_{110}+1} \\ 1 \end{pmatrix} + \ldots. \qquad \text{[S13]}$$

In the limit $u \to \infty$ (distant boundary points), the inferred eigenvalues and eigenvectors approach their noninteracting values. The u dependence of the eigenvectors and the scaled eigenvalues of the two-point correlation function are demonstrated using simulations in Fig. 3.

To fit the measured three-point correlators, we introduced three more parameters, D_{111}, D_{121}, and D_{221}. These parameters capture the leading order corrections to three-point and higher-order correlators.

Broken Detailed Balance

Let us consider the general case of Markovian dynamics, which does not satisfy Detailed Balance along a single lineage:

$$T_u(m|n) = \sum_\alpha \lambda_\alpha^u \phi_m^\alpha \psi_n^\alpha \qquad \text{[S14]}$$

with $\sum_n \phi_n^\alpha \psi_n^\beta = \delta_{\alpha\beta} \cdot \{\psi^\alpha\}$ form a nonorthogonal basis (assuming no degeneracies). If both ϕ and ψ are orthonormal basis, then it follows that, trivially, $\phi = \psi$, and detailed balance is restored.

The two-point and three-point correlators take the form,

$$\hat{G}^{(2)}_{\alpha\beta}(u) = \sum_{m,n} \psi_m^\alpha \psi_n^\beta G^{(2)}_{mn}(u) = \lambda_\alpha^u \lambda_\beta^u B_{\alpha\beta}, \qquad \text{[S15]}$$

and

$$\hat{G}^{(3)}_{\alpha\beta\gamma}(u,v) = \lambda_\alpha^u \lambda_\beta^u \lambda_\gamma^v \sum_\nu \lambda_\nu^{v-u} \tilde{C}^\nu_{\alpha\beta} B_{\nu\gamma}, \qquad \text{[S16]}$$

where $B_{\alpha\beta} = \sum_n p_n \psi_n^\alpha \psi_n^\beta$ and $\tilde{C}^\nu_{\alpha\beta} = \sum_n \phi_n^\nu \psi_n^\alpha \psi_n^\beta$ is the generalized structure constant, which is no longer fully symmetric—the fact we acknowledge by setting index ν apart from α, β. (This asymmetry reflects the directionality of the dynamics in the absence of detailed balance, distinguishing the mother state, here corresponding to index ν, from the daughters α, β.)

An observer can infer the ψ vectors and the eigenvalues λ from observing the two-point correlation functions. However, the naive structure constants constructed from the ψ in the form of the minimal model is clearly different from the actual structure constants above. The predicted three-point correlators using these structure constants would differ from the observed correlation functions.

Broken detailed balance, much like interactions, introduces "mixing" of modes. In the main text, we showed that a signature of sibling interactions was that the two-point correlator matrix $\tilde{b}_{\alpha\beta}$ was no longer diagonal. Can an observer distinguish sibling interactions from broken detailed balance by observing only the two-point correlators? With enough data, the observer can infer the ψ vectors and eigenvalues λ. If the ψ form an orthogonal basis, the dynamics were set by sibling interactions; if not, the dynamics did not satisfy detailed balance. The difference between the two cases becomes easier to spot at higher-order correlators. The structure constants for sibling interactions can be constructed from eigenvectors of two-point correlators to leading order. Structure constants under broken detailed balance, however, have a ϕ dependence (as shown above) that cannot be determined from the two-point correlation functions.

Statistical Analysis of the Experimental Data

In the main text, we showed that the eigenvalues of the transition matrix, λ_i, computed from the two-point correlation function at various distances, u, deviated from the minimal model prediction. Here, we demonstrate that this deviation is statistically significant given the finite size of our data: nine trees of nine generations.

First, we checked whether eigenvalues computed from the two-point correlation functions had predictive power given the statistical fluctuations in a finite data set. We simulated many trees of the same size as the data for random transition matrices of size 3. Fig. S2 depicts the predicted eigenvalues versus the actual ones for two-point correlation functions at different distances. The first eigenvalue is trivially 1; only the second and third eigenvalues are shown. The predictions correlate well with the actual values when the eigenvalues are large. A large eigenvalue corresponds to a long-lived fluctuation mode—see main text—and is easier to detect. Fortunately, the eigenvalues estimated from the correlation functions in the data are large enough (roughly 1, 0.8, and 0.6; see Fig. S2) to fall in the region where the predictions are well correlated with the actual values.

Fig. 2*A* depicts the departure in the measured two-point correlation functions from the prediction of the minimal model. However, deviations are expected simply due to the statistical fluctuations in the correlation functions from finite size effects. To quantify the statistical significance of the observed deviation, we simulated 10,000 iterations of nine trees of nine generations using a transition matrix deduced from the observed two-point correlation function at $u = 6$ (the starting point of the minimal model) and with no interactions. Fig. S2 shows the distribution of the third eigenvalue of the resulting two-point correlation function of these trees for different distances. The observed values from data are also shown as red arrows. The P values show that the deviation is statistically significant for distances $u = 1$ to $u = 3$.

Finite Size Fluctuations

As discussed in *Statistical Analysis of Experimental Data*, the finite size of the data imposes statistical limits on the accuracy of the correlation functions. Here, we roughly estimate the number of cells that must be observed for the correlation functions to be statistically significant. Assume that n_T trees of u generations are observed, each containing $\mathcal{N}=2^u$ cells. We would like to use this observation to compute the qth-order correlation function $G^{(q)}$.

$G^{(q)}$ is constructed from q-tuples of the leaves on the tree, the total number of which is given by $\binom{\mathcal{N}}{q} < (e\mathcal{N}/q)^q$. The qth-order correlator is a matrix with, at most, M^q independent elements, where M is the total number of states (e.g., $M=3$ in our analysis of Pvd). The correlation is also a function of at least $q-1$ distances, each of which can vary from 1 to u. A conservative estimate of the number of observations for a single element of $G^{(q)}$ at a given distance is $n_T e^q \mathcal{N}^q/(M^q q^q u^{q-1})$.

The fluctuations in the computed correlator are roughly the shot noise in the number of observations. We set this equal to the theoretical estimate of the correlator set by the transition matrix T. Denote the smallest eigenvalue of T as λ. The smallest theoretical correlation (frequency of observing a certain q-tuple) is roughly λ^{qu}. Setting this equal to the shot noise in the finite number of observations, $n_T^{1/q} \approx qM/e(\sqrt{2}\lambda)^{2u}$. The number of required trees grows exponentially with the degree of the correlation function.

Analysis of Pvd Signal in the Bulk of the Tree

We had access to the Pvd signal in the bulk of the tree from time-lapse fluorescent microscopy during the growth of the colonies. As discussed in the main text, the bulk dynamics of Pvd is more complex than the effective theory constructed using the boundary nodes. For instance, the Pvd concentration in a given bacterium can change significantly between divisions (4). Nevertheless, we set out to confirm the key attributes of the bulk dynamics that must hold for our approach to be valid. We considered fluorescence of Pvd from images taken at earlier time points (frames). The same normalization was used as for the boundary nodes (see *Methods*), but involving only the cells in the given frame. Fig. S5 shows the distribution of Pvd in the microcolony for different time points. The distribution is stationary, consistent with existence of detailed balance.

Simulations

We simulated 320,000 trees of size 6 generations using three states (phenotypes), $M=3$. The transition matrix $T(m|n)$ is a randomly chosen symmetric 3×3 matrix whose columns add to 1. We also required that the minimum eigenvalue of T be larger than 0.5 to ensure long-lasting fluctuation modes. For each tree, the root state was a uniformly drawn number from 1 to M. For noninteracting trees, at each generation, every node gives rise to two offspring. Each offspring is independently assigned color m with probability $T(m|n)$, where n is the color of the parent.

For the simulations, a random transition matrix with sibling interactions $\Gamma(m_1,m_2|n_d)$—a $3\times3\times3$ matrix—was generated. We did so by starting from a noninteracting version constructed from the randomly generated marginal distribution $T(m|n)$ (see above), $\Gamma_0(m_1,m_2|n_d)=T(m_1|n_d)T(m_2|n_d)$. An inseparable distribution was created by adding a noise term to each element of the matrix (drawn from a Gaussian distribution with mean 0 and SD 0.01), in such a way that the marginal distribution was not changed, and the symmetry condition was satisfied, $\Gamma(m_1,m_2|n_d)=\Gamma(m_2,m_1|n_d)$.

Two-point correlation function $G^{(2)}_{n_a,n_b}(u)$ was computed by counting all pairs of the final generation with colors n_a and n_b whose common ancestor is u generations back and dividing by total number of such pairs. The ordering of the pair is discarded, ensuring that matrix $G^{(2)}_{n_a,n_b}(u)$ is symmetric. Three-point correlation function $G^{(3)}_{n_a,n_b,n_c}(u,v)$ was similarly computed. The order of the closest pair is discarded, ensuring that $G^{(3)}$ is symmetric in indices n_b and n_c.

In Fig. 3*C*, we plot the difference between the predicted minimal model three-point correlators [computed using Eqs. **10** and **11** with ϕ^α_m and λ_α equal to eigenvectors of $G^{(2)}(u=6)$ and its eigenvalues to the power of 1/12, respectively] and the measured three-point correlators. For each point u and v, we have plotted the norm of the difference of the two matrices. For the interacting model, the predicted correlation functions are determined by first fitting the 3 $\tilde{b}_\alpha\beta$ to the observed two-point correlators, and fitting three $\tilde{\Gamma}(\alpha,\beta|1)$ parameters to the observed three-point correlators.

The parameters of the interacting theory were fit to the simulated/experimental data using an unconstrained nonlinear optimizer implemented using the line search algorithm (5), programmed in Matlab R2011. In Fig. 4*B*, the deviation between the predicted interaction matrix and the actual one is defined as $\Delta\tilde{\Gamma}^{(s)}=|\tilde{\Gamma}^{(s)}-\Gamma|$, where $s=0$, 1, 2 denotes, respectively, the prediction of the minimal model, fit to the second-order correlators, and the fit to second- and third-order correlators.

Hyperbolic Trees

We use the standard half-plane and Poincare disk models as representations of hyperbolic space (see, e.g., ref. 6). The Bethe lattice in hyperbolic space (Fig. 6) is constructed by creating a triangulation of the half-plane model first. The vertices of the triangulation are constructed using the Farey sequence as follows: Start with the set of fractions $\{0/1, 1/0\}$; at each iteration, add the mediant of each consecutive pair of fractions to the set [mediant of fractions a/b and c/d is $(a+b)/(c+d)$]. The first few iterations starting with $\{0/1, 1/0\}$ result in sets: $\{0/1, 1/1, 1/0\}$, $\{0/1, 1/2, 1/1, 2/1, 1/0\}$, $\{0/1, 1/3, 1/2, 2/3, 1/1, 3/2, 2/1, 3/1, 1/0\}$, etc. Each new element in the set is a new vertex (on the real line) that is connected by geodesics in the half-plane to its two parent vertices. The Bethe lattice is the dual of the triangulation constructed by drawing the geodesics connecting the centroids of neighboring triangles.

The resulting triangulation and Bethe lattice in the half-plane is mapped onto the Poincare disk using the standard transformation (6) (see Fig. S5),

$$z \to \frac{z-i}{iz-1}. \qquad \textbf{[S17]}$$

Transformations of the following form (known as Mobius transformations) are isometries of hyperbolic space and map the Poincare disk onto itself (6):

$$z \to \frac{\alpha z+\beta}{\overline{\beta} z+\overline{\alpha}}, \qquad \textbf{[S18]}$$

where $\alpha,\beta\in\mathbb{C}$ and $|\alpha|^2-|\beta|^2=1$. For the transformation shown in Fig. 6*B*, we repeatedly applied the infinitesimal transformation, $\alpha=1-i\epsilon$ and $\beta=-\epsilon$. This transformation maps the tree onto itself but effectively shifts the origin by one node. We used the same transformation on the Farey triangulation to move one node to the origin of the Poincare disk, obtaining the threefold symmetry. Designating a particular node as the origin is an arbitrary choice with no bearing on the correlation functions. Therefore, correlation functions on a tree are invariant under the above transformation.

1. Harlow D, Shenker S, Stanford D, Susskind L, Eternal symmetree, arXiv:1110.0496.
2. Itzykson C, Drouffe JM (1989) *Statistical Field Theory* (Cambridge Univ Press, Cambridge, UK).
3. DiFrancesco P, Mathieu P, Senechal D (1999) *Conformal Field Theory* (Springer, New York).
4. Julou T, et al. (2013) Cell-cell contacts confine public goods diffusion inside *Pseudomonas aeruginosa* clonal microcolonies. *Proc Natl Acad Sci USA* 110(31): 12577–12582.
5. Fletcher R (1987) *Practical Methods of Optimization* (Wiley, New York).
6. Anderson JW (2005) *Hyperbolic Geometry* (Springer, London).

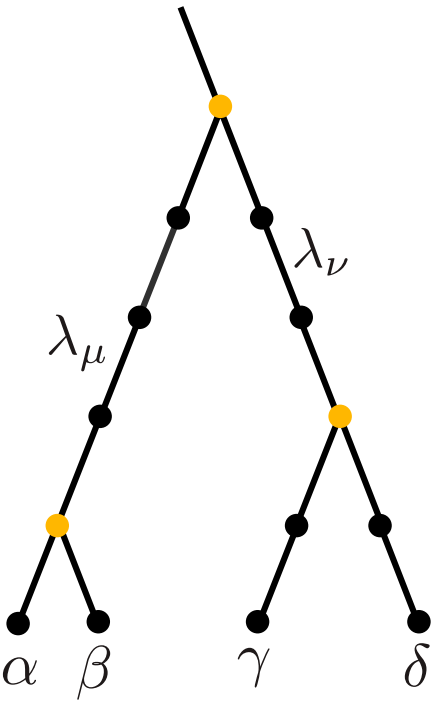

Fig. S1. Calculating a correlation function. Four points on the boundary are considered. We are interested in observing modes α, β, γ, and δ on the boundary with the genealogical distances shown in the figure. For example, α and β are observed in siblings. Each edge picks up a factor λ_i, where i is the mode propagating along the edge. Vertices with three edges (light color) pick up a factor of a structure constant. We sum over all possible propagation modes between internal vertices, μ and ν, as shown. The input vector into the common ancestor of all four points is the equilibrium mode, $\alpha = 0$.

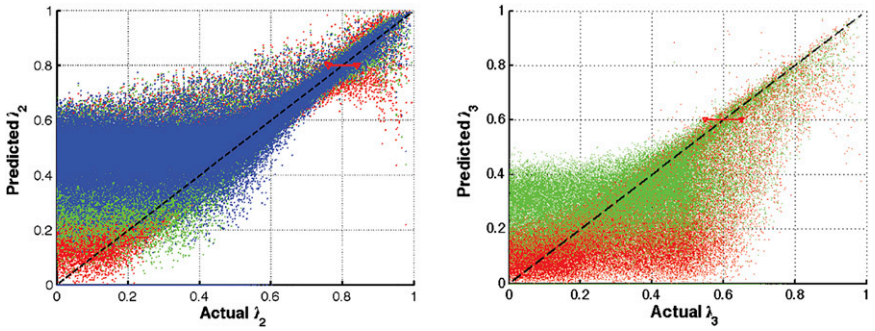

Fig. S2. Simulated trees with random transition matrices. Predicted versus actual eigenvalues (second and third; *Left* and *Right*, respectively) for simulated trees with random transition matrices that satisfy detailed balance and have no interactions. The colors denote the distance u at which the two-point correlation function is used to estimate the eigenvalues; blue, green, and red correspond to $u = 1$, $u = 2$, and $u = 3$, respectively. The red arrows show the eigenvalues estimated from the data. The small eigenvalues have almost no predictive power, since the amplitude of their corresponding propagation mode is smaller than the statistical fluctuations.

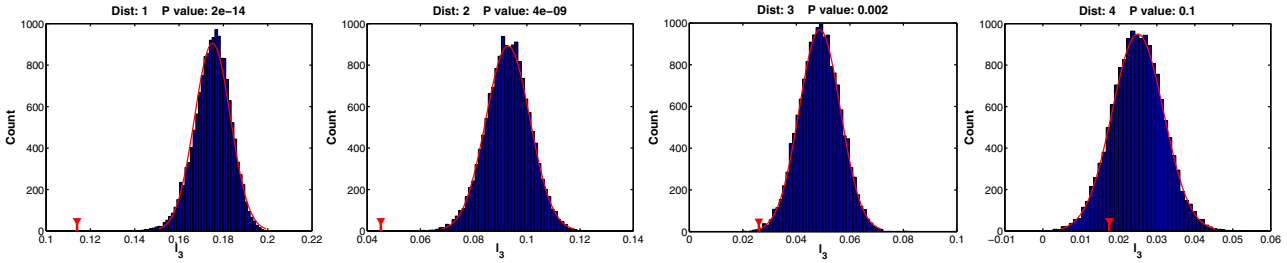

Fig. S3. Statistical significance of the deviation in the observed two-point correlation functions from that of the null-hypothesis. Histogram of the third eigenvalue of the two-point correlation matrix of simulated trees with the same transition matrix as the null-hypothesis minimal model, for distances $u = 1$ (*Left*), $u = 2$ (*Center Left*), $u = 3$ (*Center Right*), and $u = 4$ (*Right*). The red arrow shows the value from the measured two-point correlation function of the data. The *P* values are shown at the top.

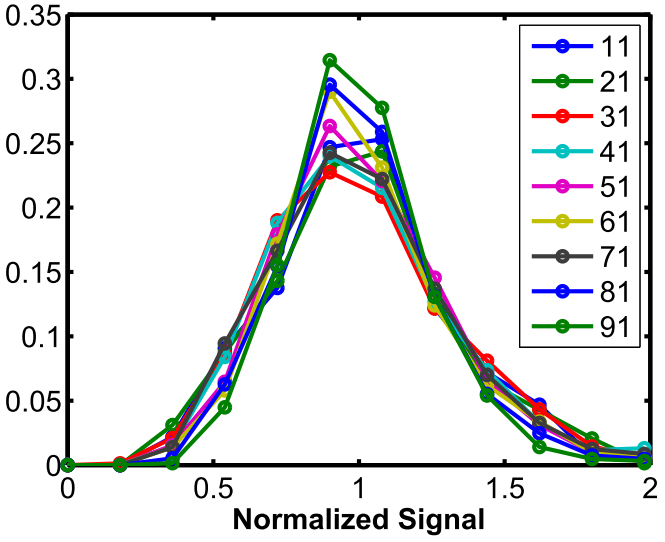

Fig. S4. Distribution of the Pvd signal of all cells in a given frame (time point) averaged over 10 adjacent frames and all nine trees of the data. The key shows the frame number. Each generation is roughly 10 frames. The distribution is stationary.

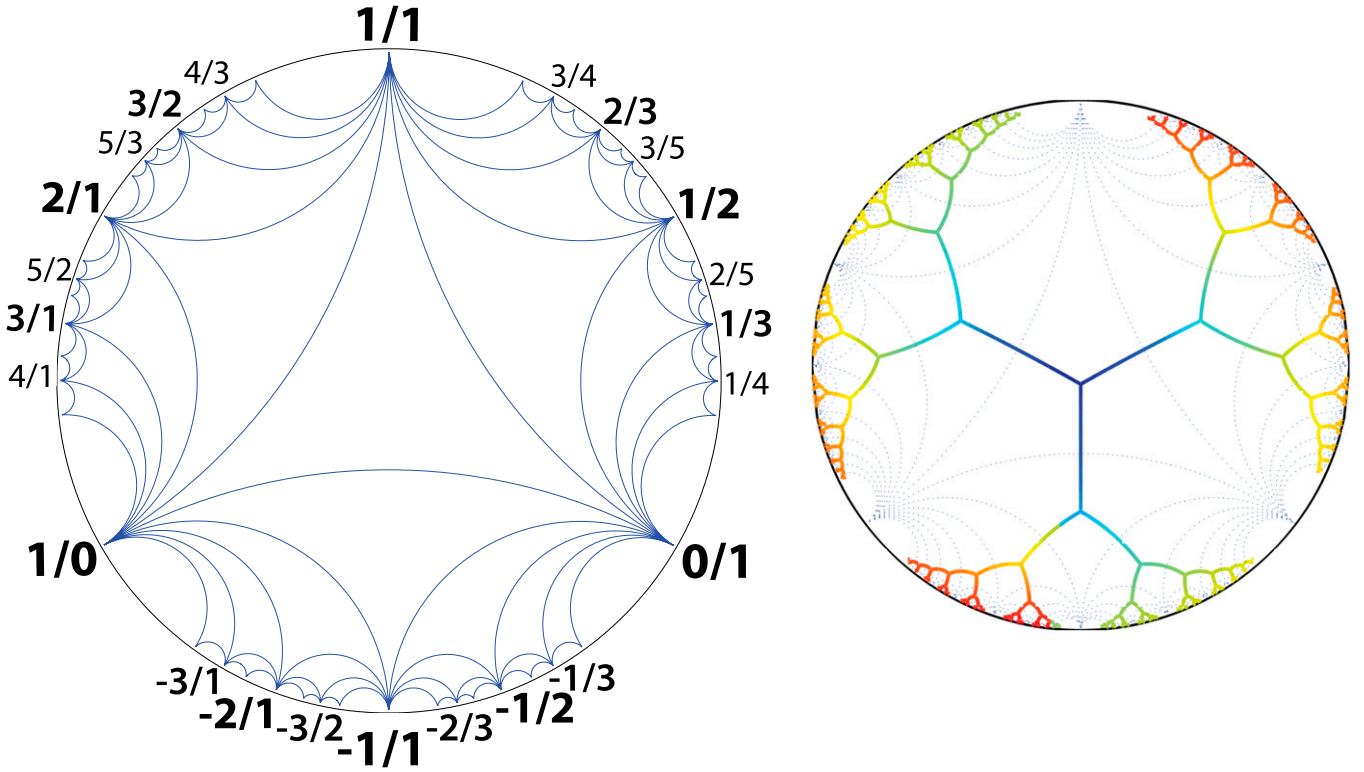

Fig. S5. Bethe lattice in the Poincare disk. (*Left*) Triangulation of the hyperbolic space in the Poincare disk representation using the Farey sequence construction. The fractions show how the Farey sequence divides up the unit circle boundary into smaller segments (this is a mapping of the real line to the boundary of the disk). Size of the font is reduced at each consecutive iteration of the Farey construct. (*Right*) The Bethe lattice is the dual to the triangulation and is constructed by drawing the geodesics connecting the centroids of neighboring triangles. The coloring scheme is a guide for the eyes.